Bound States in the Continuum through Environmental Design

Alexander Cerjan,[1,*] Chia Wei Hsu,[2] and Mikael C. Rechtsman[1]
[1]Department of Physics, The Pennsylvania State University, University Park, Pennsylvania 16802, USA
[2]Ming Hsieh Department of Electrical Engineering, University of Southern California, Los Angeles, California 90089, USA

(Received 21 January 2019; revised manuscript received 11 April 2019; published 10 July 2019)

We propose a new paradigm for realizing bound states in the continuum (BICs) by engineering the environment of a system to control the number of available radiation channels. Using this method, we demonstrate that a photonic crystal slab embedded in a photonic crystal environment can exhibit both isolated points and lines of BICs in different regions of its Brillouin zone. Finally, we demonstrate that the intersection between a line of BICs and a line of leaky resonances can yield exceptional points connected by a bulk Fermi arc. The ability to design the environment of a system opens up a broad range of experimental possibilities for realizing BICs in three-dimensional geometries, such as in 3D-printed structures and the planar grain boundaries of self-assembled systems.

DOI: 10.1103/PhysRevLett.123.023902

Bound states in the continuum (BICs), which are radiationless states in an open system whose frequency resides within the band of radiative channels, have recently attracted a great deal of interest for their applications in producing vector beams from surface emitting lasers [1–8] and enhancing the resolution of certain classes of sensors [9–11]. Originally proposed in 1929 in a quantum mechanical context [12], BICs have now been found in a broad range of physical systems, such as photonic crystal slabs [13–25], waveguide arrays [26–28], strongly coupled plasmonic-photonic systems [29], metasurfaces [30,31], acoustics [32–37], and water waves [38–43]. Additionally, lines of BICs were recently found in composite birefringent structures [44,45]. In principle, BICs can be classified into three main categories [46]: those which are engineered using an inverse construction method, those which are protected by symmetry or separability, and those which can be found "accidentally" through tuning a system's parameters. In practice, however, systems supporting BICs from the first category are difficult to experimentally realize due to the high degree of fine-tuning required. Thus, much of the current excitement surrounding BICs has focused on systems which feature symmetry-protected and accidental BICs; moreover, these BICs have been shown to possess topological protection that guarantees their existence under perturbations to the system [20,45,47–51].

Traditionally, the appearance of accidental BICs is understood in terms of modal interference [22,46,52], with two or more resonances of the device destructively interfering in the system's radiation channels yielding a bound mode spatially localized to the device. This interpretation emphasizes how tuning the device's parameters changes the spatial profiles of its resonances to realize this modal interference, while considering the available radiation channels in the surrounding environment as fixed. This is because most previously studied systems with accidental BICs consider devices embedded in free space, where the outgoing propagating channels cannot be readily altered. However, from this argument it is clear that the environment is also important in determining the presence or absence of BICs: the environment's properties dictate the number and modal profiles of the available radiation channels, and thus strongly constrain when it is possible to achieve the necessary modal interference. Yet thus far, the role of the environment in creating BICs has remained relatively unexplored.

In this Letter, we show that the properties of the environment play an important role in determining where BICs can exist, as much as the specific geometry of the device embedded in this environment. This argument is presented using coupled-mode theory (CMT) [53–55] and as such is completely general and applicable to all systems which exhibit BICs. As an example of this theory, we then show that by embedding a photonic crystal slab into a photonic crystal environment, both isolated BICs and lines of BICs can be found in the resonance bands of the photonic crystal slab depending on the number of available radiation channels. Moreover, perturbations to the environment can shift the locations of the system's BICs even when the photonic crystal slab layer remains unchanged, demonstrating that the environment of a system is an equal partner to the embedded device in determining the existence and types of BICs found in the system. Finally, we show that when two resonance bands of the photonic crystal slab undergo a symmetry-protected band crossing, it is possible for a line of BICs to pass from one band to the other through a bulk Fermi arc. Understanding the relationship between the device and surrounding environment in forming BICs is a necessary first step towards realizing BICs in three-dimensional geometries, such as grain

boundaries in photonic crystals [56] or self-assembled structures [57].

To illuminate the role of the environment in determining the presence and properties of BICs in a system, we first consider a photonic crystal slab embedded in an environment, such that the entire system is periodic in the transverse plane. For any choice of in-plane wave vector $\mathbf{k}_\parallel = (k_x, k_y)$ and frequency ω, the outgoing field can be written as a sum of the incoming and scattered fields $\mathbf{E}_{\text{out}}(\mathbf{x};\mathbf{k}) = \mathbf{E}_{\text{in}}(\mathbf{x};\mathbf{k}) + \mathbf{E}_{\text{res}}(\mathbf{x};\mathbf{k})$. The incoming and outgoing fields can be expressed in the basis of the environmental channels $\mathbf{E}_{\text{in}}(\mathbf{x};\mathbf{k}) = \sum_n s_{\text{in},n} e^{-ik_{z,n}|z|}\mathbf{e}_{\text{in},n}(\mathbf{x};\mathbf{k})$ and $\mathbf{E}_{\text{out}}(\mathbf{x};\mathbf{k}) = \sum_n s_{\text{out},n} e^{ik_{z,n}|z|}\mathbf{e}_{\text{out},n}(\mathbf{x};\mathbf{k})$ in which $s_{\text{in/out},n}$ is the complex amplitude of the channel mode $\mathbf{e}_{\text{in/out},n}$ traveling towards or away from the photonic crystal slab with wave vector $k_{z,n}$. The field resonantly scattered by the photonic crystal slab can be expressed in terms of the resonances (also called quasinormal modes) of the slab $\mathbf{E}_{\text{res}}(\mathbf{x};\mathbf{k}) = \sum_j a_j \mathcal{E}_{\text{res},j}(\mathbf{x};\mathbf{k}_\parallel)$, which satisfy radiating boundary conditions in z and have complex frequencies $\tilde{\omega}_j = \omega_j + i\gamma_j$ [55]. Focusing now on a single isolated resonance a_0 with frequency $\tilde{\omega}_0$, from the linearity of Maxwell's equations these modal amplitudes can be related using CMT

$$-i\omega a_0 = -(i\omega_0 + \gamma_0)a_0 + K^T s_{\text{in}}, \tag{1}$$

$$s_{\text{out}} = C s_{\text{in}} + D a_0, \tag{2}$$

in which $C \in \mathbb{C}^{N\times N}$ represents the direct transmission and reflection through the photonic crystal slab, $K = D \in \mathbb{C}^{N\times 1}$ gives the coupling of the resonance to the available radiation channels for the reciprocal systems without material loss considered here, and N is the total number of radiative channels at ω. If the system possesses 180° rotational symmetry about the z axis (C_2), such that $-\mathbf{k}_\parallel$ is equivalent to $\mathbf{k}_\parallel$, by time-reversal symmetry C and D can be shown to be related as [54]

$$CD^* = -D. \tag{3}$$

In the language of CMT, a BIC occurs when $D = 0$; i.e., all of the outcoupling coefficients of the resonance to all of the available radiation channels are simultaneously zero. For this to occur accidentally with finite probability, there must be at least as many degrees of freedom of the system as there are unknown parameters of D. Thus, naively one would expect to require $2N$ degrees of freedom to find BICs for the N complex coefficients comprising D. However, while the resonance outcoupling coefficients D are dependent upon the specific patterning of the slab, the direct scattering processes C are agnostic to this patterning and can instead be considered using a homogeneous dielectric slab [16,58]. As such, C is essentially constant for perturbations to the photonic crystal slab and Eq. (3) represents a set of additional constraints on D, halving its number of unknown parameters. Thus, if an entire system is C_2 symmetric, one only needs N degrees of freedom to find accidental BICs.

A second symmetry commonly present in photonic crystal slab systems is mirror symmetry about the $z = 0$ plane (σ_z). Although this symmetry is not required to find BICs, its presence further reduces the number of unknown parameters among the components of D as the outcoupling coefficients d_m,d_n, form mirror-symmetric pairs $d_n = \sigma d_m$ with $\sigma = \pm 1$ depending on the symmetry of the resonance about $z = 0$ [59]. Thus, mirror symmetry both halves the number of unknown parameters in D and also halves the number of independent constraints represented by Eq. (3).

To provide an explicit example of how to use these constraints to find BICs, consider the photonic crystal slab embedded in a photonic crystal environment shown in Fig. 1(a). The presence of the photonic crystal environment breaks the degeneracy between the two polarizations of

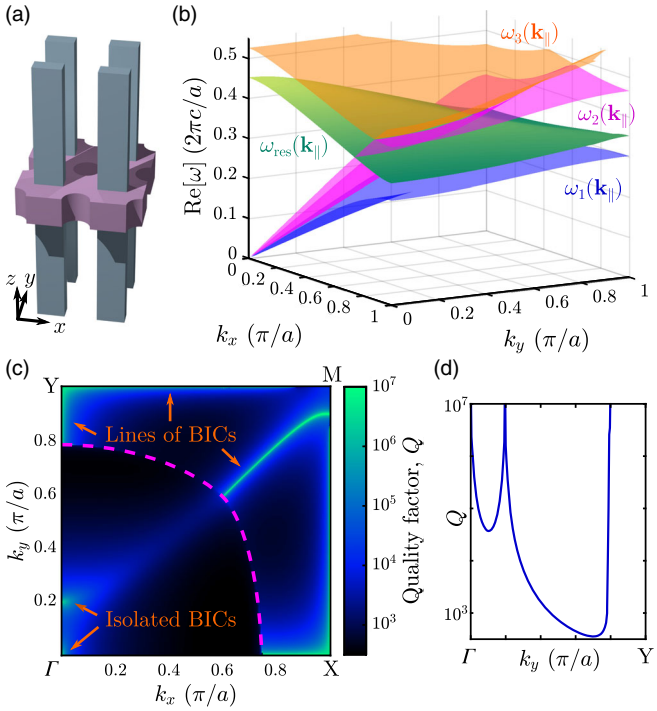

FIG. 1. (a) Schematic of a photonic crystal slab embedded in a C_{2v} symmetric photonic crystal environment of infinitely tall dielectric rectangles (the rectangles in the environment do not penetrate into the slab). The rectangles have length and width $l_{\text{env}} = w_{\text{env}}/2 = 0.23a$ and dielectric permittivity $\varepsilon_{\text{env}} = 12$, while the slab has height $h_{\text{slab}} = 0.5a$, holes with radius $r_{\text{slab}} = 0.22a$, and dielectric permittivity $\varepsilon_{\text{slab}} = 7$, where a is the lattice constant of the system. (b) Photonic band structure of the slab resonances, $\omega_{\text{res}}(\mathbf{k}_\parallel)$ (green), and the first three low-frequency cutoffs of the radiation channels, $\omega_n(\mathbf{k}_\parallel)$ (blue, purple, and orange). (c) Quality factor of the photonic crystal slab resonances as a function of $\mathbf{k}_\parallel$ calculated using MEEP [61]. Lines of BICs are seen for portions of Γ–X, Γ–Y, X–M, Y–M, and near Γ–M, where only one environmental channel is present, outside the dashed purple line. Here $\Gamma = (0,0)$, $X = (1,0)$, $Y = (0,1)$, and $M = (1,1)$. (d) Quality factor along Γ–Y showing two isolated BICs at Γ and near $\mathbf{k}_\parallel = (0, 0.2\pi/a)$ where there are two radiative channels.

light in homogeneous media, splitting the light line $\omega = c|\mathbf{k}_\parallel|$ into separate frequency cutoff bands $\omega_n(\mathbf{k}_\parallel)$, below which the nth radiative channel does not exist [60]. As such, for the transverse electric (TE)-like resonance band of the photonic crystal slab shown in Fig. 1(b), the central region of this band in the Brillouin zone [inside the dashed purple line in Fig. 1(c)] can couple to two radiation channels on each side of the slab, while the exterior region of the resonance band can only couple to a single radiation channel on each side. In other words, the photonic crystal "cladding" can reduce the number of available radiation channels in parts of the Brillouin zone.

First consider the single-radiation-channel region outside the dashed purple line in Fig. 1(c). Here, there initially appear to be 4 unknown parameters in $D = (d_{\text{above}}, d_{\text{below}})^T$. However, as the system is mirror symmetric about $z = 0$ and the resonance band's states are even under this symmetry, $D = d_0(1,1)^T$, with d_0 being the remaining complex free parameter. Moreover, one can show that the constraint represented by Eq. (3) in this region can be written as

$$d_0^*(r + t) = -d_0, \tag{4}$$

which amounts to a constraint on the phase of d_0, as $|r|^2 + |t|^2 = 1$, where r and t are the direct transmission and reflection coefficients and $C = (r, t; t, r)$. Thus, in this region there is only a single unknown parameter in D, and as there are 2 degrees of freedom in the system, k_x and k_y, lines of BICs can be found in the resonance band in the single-radiation-channel region along portions of the edge of the Brillouin zone, as well as near portions of the Γ–M line, as shown in Fig. 1(c). These lines of BICs can be viewed as 1D topological defects, similar to domain walls in spin-flip systems, across which angle(d_0) jumps by π [62]. Although the CMT analysis presented here does not guarantee $D = 0$, a suitable choice of gauge using Eq. (4) allows for $d_0 \in \mathbb{R}$, and in this gauge d_0 changes sign across the lines of BICs, guaranteeing $D = 0$ [62].

In the two-radiation-channel region, one finds that D has two unknown parameters, and thus it is possible to find isolated accidental BICs, similar to those found in previous works of photonic crystal slabs embedded in homogeneous media [18,20]. For the system shown in Fig. 1(a), there is an accidental BIC near $\mathbf{k}_\parallel = (0, 0.2)\pi/a$, and a symmetry protected BIC at Γ where both radiative channels are even under C_2 but the resonance band is odd, as marked in Fig. 1(c).

To demonstrate that the environment is an equal partner to the resonant device in determining the presence of BICs, we increase the symmetry of the photonic crystal environment (C_{4v} as opposed to C_{2v}) but preserve the same photonic crystal slab, as shown in Fig. 2(a). Thus, although the frequencies and spatial profiles of the resonances of the photonic crystal slab remain the same, where they achieve complete destructive interference in the radiation channels

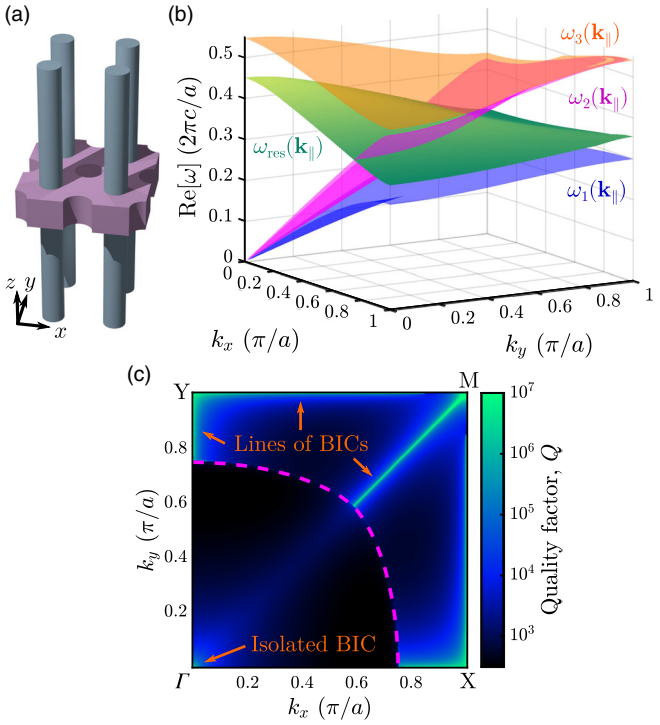

FIG. 2. (a) Schematic of a photonic crystal slab embedded in a C_{4v} symmetric photonic crystal environment of infinitely tall dielectric cylinders. The rods have radius $r_{\text{env}} = 0.18a$ and dielectric $\varepsilon_{\text{env}} = 12$, while the slab has height $h_{\text{slab}} = 0.5a$, holes with radius $r_{\text{slab}} = 0.22a$, and dielectric $\varepsilon_{\text{slab}} = 7$, where a is the lattice constant of the system. (b) Photonic band structure, with the same conventions as Fig. 1(b). (c) Quality factor of the photonic crystal slab resonances as a function of $\mathbf{k}_\parallel$. Lines of BICs are seen in the one-radiation-channel region outside the dashed purple line, while an isolated BIC is seen at Γ.

of the new environment has changed. This shift can be seen by comparing the distribution of BICs found in Fig. 2(c), to the distribution seen in Fig. 1(c). In the C_{4v} symmetric environment, the isolated accidental BIC in the two-radiation-channel region [of the C_{2v} structure—see Fig. 1(c)] has merged with the isolated BIC at Γ, similar to the merging of BICs described by Zhen *et al.* [20] and the line of accidental BICs near the Γ–M line has shifted to lie exactly along Γ–M and become protected by mirror symmetry about the $x = y$ line.

There is a curious feature of the lines of BICs along X–M and Y–M found in both Figs. 1(c) and 2(c): the lines of BICs appear to abruptly terminate prior to reaching M. Although such a termination is not precluded by the coupled-mode analysis previously discussed, the lines of BICs along X–M and Y–M are not accidental but are instead protected by symmetry, as the resonance band is odd about the $x = 0$ ($y = 0$) plane along this portion of the X–M (Y–M) high symmetry line, while the radiative channel is even about the same plane, as shown in Figs. 3(c) and 3(e). Thus, as the symmetry of the system has not changed at these points along high symmetry lines,

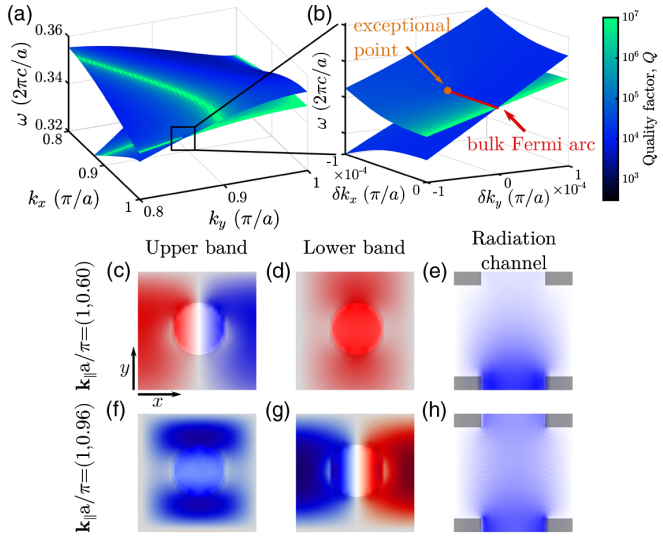

FIG. 3. (a) Frequencies and quality factors near M for two TE-like resonance bands of the photonic crystal slab and C_{2v} symmetric photonic crystal environment shown in Fig. 1(a). There are two bulk Fermi arcs at $\mathbf{k}_{\parallel}a/\pi = (1, 0.852)$ and $\mathbf{k}_{\parallel}a/\pi = (0.872, 1)$. (b) Model showing the bulk Fermi arc at $\mathbf{k}_{\parallel}a/\pi = (1, 0.852)$. (c)–(h) Cross section of the E_x component in the xy plane of the Bloch mode profiles of the upper resonance band (c), lower resonance band (d), and radiation channel (e) at $\mathbf{k}_{\parallel}a/\pi = (1, 0.6)$. Locations of the dielectric features in the photonic crystal slab (c)–(d) or photonic crystal environment (e) are denoted with light gray shading. (f)–(h) Similar to (c)–(e), except at $\mathbf{k}_{\parallel}a/\pi = (1, 0.96)$. Mode profiles of the resonance bands were calculated using MEEP [61], while the radiation channel profiles were calculated using MPB [63].

it is strange that the modal profile of the resonance band would suddenly change to allow for the state to couple to the radiative channel. However, the disappearance of the line of BICs from the resonance band coincides with the location of an intersection with a second TE-like resonance band of the photonic crystal slab, shown in Figs. 3(a)–3(b). Elsewhere in the Brillouin zone these two resonance bands couple and exhibit an avoided crossing, but along the high symmetry line X–M (Y–M) these two bands have opposite mirror symmetry about the $x = 0$ ($y = 0$) plane of the system, as shown in Figs. 3(c) and 3(d), and thus exhibit a band crossing.

If the coupling to the radiative channels could be ignored such that the system were completely Hermitian, this accidental band crossing would occur at a Dirac point. Instead, the coupling of the resonance bands to the outgoing radiative channels results in this system being non-Hermitian. Moreover, the two resonance bands in question couple to the single available radiative channel at different rates; i.e., one resonance band possesses a line of symmetry-protected BICs while the other resonance does not. Because of this unequal radiative coupling, where the hypothetical nonradiating Hermitian system would possess a Dirac point connecting the two bands, these two resonance bands are instead joined by a bulk Fermi arc in the radiating non-Hermitian system [64]. Bulk Fermi arcs occur generically in non-Hermitian systems and form when a Dirac point is split into two exceptional points [65] connected by a contour where the real part of the frequencies of the two resonance bands are equal, $\mathrm{Re}[\omega_+] = \mathrm{Re}[\omega_-]$. When two bands are joined at a bulk Fermi arc, they form two halves of a single Riemann surface.

In the vicinity of the bulk Fermi arc, the effective Hamiltonian for the systems considered here is

$$\hat{H} = \omega_D - i\gamma + (v_{gy}\delta k_y - i\gamma)\hat{\sigma}_z + v_{gx}\delta k_x\hat{\sigma}_x, \tag{5}$$

which results in the spectrum of the resonance bands

$$\omega_\pm = \omega_D - i\gamma \pm \sqrt{v_{gx}^2\delta k_x^2 + v_{gy}^2\delta k_y^2 - \gamma^2 - 2i\gamma v_{gy}\delta k_y}. \tag{6}$$

Here, $(\delta k_x, \delta k_y)$ is the wave vector displacements from the underlying Dirac point at $\mathbf{k}_{\parallel,D}$ which has frequency ω_D, 2γ is the radiative rate of the resonance band which couples to the single environmental channel, (v_{gx}, v_{gy}) is the group velocity describing the dispersion near the Dirac point, and $\hat{\sigma}_{x,z}$ are Pauli matrices. Equations (5) and (6) are written for the accidental band crossing along X–M, but letting $x \leftrightarrow y$ yields the correct set of equations for the accidental band crossing along Y–M. As can be seen, the spectrum given in Eq. (6) exhibits a pair of exceptional points at $(\delta k_x, \delta k_y) = (\pm\gamma/v_{gx}, 0)$, where $\omega_+ = \omega_-$, and which are connected by a bulk Fermi arc along the contour $\delta k_x < |\gamma/v_{gx}|$ and $\delta k_y = 0$.

The connection between the two resonance bands at the bulk Fermi arc explains the apparent abrupt termination of the lines of BICs in Figs. 1(c) and 2(c). Along the X–M high symmetry lines where $\delta k_x = 0$, one resonance band remains a BIC with $\mathrm{Im}[\omega] = 0$, but which band possesses the BIC switches when the line of BICs passes through the bulk Fermi arc, where the two bands are joined and form a single Riemann surface, as shown in Figs. 3(a) and 3(b). We can confirm that near M the symmetry of the upper and lower bands switches along the X–M line upon passing through the bulk Fermi arc by viewing the modal profiles of the resonances on both sides of it. As can be seen in Figs. 3(c)–3(h), for $\delta k_y < 0$, the odd x symmetry mode is found on the upper resonance band, but for $\delta k_y > 0$ this mode is found on the lower resonance band. Thus, the symmetry protected line of BICs does exist along the entire high symmetry line but passes from the upper resonance band to the lower resonance band through a bulk Fermi arc.

In conclusion, we have demonstrated that the environment surrounding a device is an equal partner in determining the presence of BICs. This ability to engineer the environment rather than the device to realize BICs in a system opens up a broad range of new experimental

possibilities. First, given the advent of advanced 3D-printing techniques such as two-photon polymerization technology [56], we expect that structures such as the one described here can be straightforwardly fabricated in photonic systems. Likewise, conventional 3D-printing already enables the construction of acoustic systems with complex unit cells [66,67] which could be used to realize BICs through environmental design. Moreover, there are many photonic systems, such as planar grain boundaries in self-assembled structures [57], where controlling the specifics of the embedded device may be very difficult, but engineering the environment is comparatively simple, that may yield an entirely different route to photonic BICs than has been previously studied.

The authors acknowledge support from the National Science Foundation under Grants No. ECCS-1509546 and No. DMS-1620422 as well as the Charles E. Kaufman foundation under Grant No. KA2017-91788.

*awc19@psu.edu

[1] M. Meier, A. Mekis, A. Dodabalapur, A. Timko, R. E. Slusher, J. D. Joannopoulos, and O. Nalamasu, Laser action from two-dimensional distributed feedback in photonic crystals, Appl. Phys. Lett. **74**, 7 (1999).

[2] M. Imada, S. Noda, A. Chutinan, T. Tokuda, M. Murata, and G. Sasaki, Coherent two-dimensional lasing action in surface-emitting laser with triangular-lattice photonic crystal structure, Appl. Phys. Lett. **75**, 316 (1999).

[3] S. Noda, M. Yokoyama, M. Imada, A. Chutinan, and M. Mochizuki, Polarization mode control of two-dimensional photonic crystal laser by unit cell structure design, Science **293**, 1123 (2001).

[4] E. Miyai, K. Sakai, T. Okano, W. Kunishi, D. Ohnishi, and S. Noda, Photonics: Lasers producing tailored beams, Nature (London) **441**, 946 (2006).

[5] H. Matsubara, S. Yoshimoto, H. Saito, Y. Jianglin, Y. Tanaka, and S. Noda, GaN photonic-crystal surface-emitting laser at blue-violet wavelengths, Science **319**, 445 (2008).

[6] S. Iwahashi, Y. Kurosaka, K. Sakai, K. Kitamura, N. Takayama, and S. Noda, Higher-order vector beams produced by photonic-crystal lasers, Opt. Express **19**, 11963 (2011).

[7] K. Kitamura, K. Sakai, N. Takayama, M. Nishimoto, and S. Noda, Focusing properties of vector vortex beams emitted by photonic-crystal lasers, Opt. Lett. **37**, 2421 (2012).

[8] K. Hirose, Y. Liang, Y. Kurosaka, A. Watanabe, T. Sugiyama, and S. Noda, Watt-class high-power, high-beam-quality photonic-crystal lasers, Nat. Photonics **8**, 406 (2014).

[9] A. A. Yanik, A. E. Cetin, M. Huang, A. Artar, S. Hossein Mousavi, A. Khanikaev, J. H. Connor, G. Shvets, and H. Altug, Seeing protein monolayers with naked eye through plasmonic Fano resonances, Proc. Natl. Acad. Sci. U.S.A. **108**, 11784 (2011).

[10] B. Zhen, S.-L. Chua, J. Lee, A. W. Rodriguez, X. Liang, S. G. Johnson, J. D. Joannopoulos, M. Soljačić, and O. Shapira, Enabling enhanced emission and low-threshold lasing of organic molecules using special Fano resonances of macroscopic photonic crystals, Proc. Natl. Acad. Sci. U.S.A. **110**, 13711 (2013).

[11] S. Romano, G. Zito, S. Torino, G. Calafiore, E. Penzo, G. Coppola, S. Cabrini, I. Rendina, and V. Mocella, Label-free sensing of ultralow-weight molecules with all-dielectric metasurfaces supporting bound states in the continuum, Photonics Res. **6**, 726 (2018).

[12] J. von Neumann and E. Wigner, Über merkwürdige diskrete eigenwerte, Phys. Z. **30**, 465 (1929).

[13] P. Paddon and J. F. Young, Two-dimensional vector-coupled-mode theory for textured planar waveguides, Phys. Rev. B **61**, 2090 (2000).

[14] V. Pacradouni, W. J. Mandeville, A. R. Cowan, P. Paddon, J. F. Young, and S. R. Johnson, Photonic band structure of dielectric membranes periodically textured in two dimensions, Phys. Rev. B **62**, 4204 (2000).

[15] T. Ochiai and K. Sakoda, Dispersion relation and optical transmittance of a hexagonal photonic crystal slab, Phys. Rev. B **63**, 125107 (2001).

[16] S. Fan and J. D. Joannopoulos, Analysis of guided resonances in photonic crystal slabs, Phys. Rev. B **65**, 235112 (2002).

[17] C. Wei Hsu, B. Zhen, S.-L. Chua, S. G. Johnson, J. D. Joannopoulos, and M. Soljačić, Bloch surface eigenstates within the radiation continuum, Light Sci. Appl. **2**, e84 (2013).

[18] C. Wei Hsu, B. Zhen, J. Lee, S.-L. Chua, S. G. Johnson, J. D. Joannopoulos, and M. Soljačić, Observation of trapped light within the radiation continuum, Nature (London) **499**, 188 (2013).

[19] Y. Yang, C. Peng, Y. Liang, Z. Li, and S. Noda, Analytical Perspective for Bound States in the Continuum in Photonic Crystal Slabs, Phys. Rev. Lett. **113**, 037401 (2014).

[20] B. Zhen, C. W. Hsu, L. Lu, A. D. Stone, and M. Soljačić, Topological Nature of Optical Bound States in the Continuum, Phys. Rev. Lett. **113**, 257401 (2014).

[21] H. Zhou, B. Zhen, C. Wei Hsu, O. D. Miller, S. G. Johnson, J. D. Joannopoulos, and M. Soljačić, Perfect single-sided radiation and absorption without mirrors, Optica **3**, 1079 (2016).

[22] X. Gao, C. Wei Hsu, B. Zhen, X. Lin, J. D. Joannopoulos, M. Soljačić, and H. Chen, Formation mechanism of guided resonances and bound states in the continuum in photonic crystal slabs, Sci. Rep. **6**, 31908 (2016).

[23] A. Kodigala, T. Lepetit, Q. Gu, B. Bahari, Y. Fainman, and B. Kanté, Lasing action from photonic bound states in continuum, Nature (London) **541**, 196 (2017).

[24] W. Zhang, A. Charous, M. Nagai, D. M. Mittleman, and R. Mendis, Extraordinary optical reflection resonances and bound states in the continuum from a periodic array of thin metal plates, Opt. Express **26**, 13195 (2018).

[25] M. Minkov, I. A. D. Williamson, M. Xiao, and S. Fan, Zero-Index Bound States in the Continuum, Phys. Rev. Lett. **121**, 263901 (2018).

[26] Y. Plotnik, O. Peleg, F. Dreisow, M. Heinrich, S. Nolte, A. Szameit, and M. Segev, Experimental Observation of Optical Bound States in the Continuum, Phys. Rev. Lett. **107**, 183901 (2011).

[27] S. Weimann, Y. Xu, R. Keil, A. E. Miroshnichenko, A. Tünnermann, S. Nolte, A. A. Sukhorukov, A. Szameit, and Y. S. Kivshar, Compact Surface Fano States Embedded in the Continuum of Waveguide Arrays, Phys. Rev. Lett. **111**, 240403 (2013).

[28] G. Corrielli, G. Della Valle, A. Crespi, R. Osellame, and S. Longhi, Observation of Surface States with Algebraic Localization, Phys. Rev. Lett. **111**, 220403 (2013).

[29] S. I. Azzam, V. M. Shalaev, A. Boltasseva, and A. V. Kildishev, Formation of Bound States in the Continuum in Hybrid Plasmonic-Photonic Systems, Phys. Rev. Lett. **121**, 253901 (2018).

[30] K. Koshelev, S. Lepeshov, M. Liu, A. Bogdanov, and Y. Kivshar, Asymmetric Metasurfaces with High-Q Resonances Governed by Bound States in the Continuum, Phys. Rev. Lett. **121**, 193903 (2018).

[31] K. Koshelev, A. Bogdanov, and Y. Kivshar, Meta-optics and bound states in the continuum, arXiv:1810.08698.

[32] R. Parker, Resonance effects in wake shedding from parallel plates: Some experimental observations, J. Sound Vib. **4**, 62 (1966).

[33] R. Parker, Resonance effects in wake shedding from parallel plates: Calculation of resonant frequencies, J. Sound Vib. **5**, 330 (1967).

[34] N. A. Cumpsty and D. S. Whitehead, The excitation of acoustic resonances by vortex shedding, J. Sound Vib. **18**, 353 (1971).

[35] W. Koch, Resonant acoustic frequencies of flat plate cascades, J. Sound Vib. **88**, 233 (1983).

[36] R. Parker and S. A. T. Stoneman, The excitation and consequences of acoustic resonances in enclosed fluid flow around solid bodies, Proc. Inst. Mech. Eng. C **203**, 9 (1989).

[37] D. V. Evans, M. Levitin, and D. Vassiliev, Existence theorems for trapped modes, J. Fluid Mech. **261**, 21 (1994).

[38] F. Ursell, Trapping modes in the theory of surface waves, Math. Proc. Cambridge Philos. Soc. **47**, 347 (1951).

[39] D. S. Jones, The eigenvalues of $\nabla^2 u + \lambda u = 0$ when the boundary conditions are given on semi-infinite domains, Math. Proc. Cambridge Philos. Soc. **49**, 668 (1953).

[40] M. Callan, C. M. Linton, and D. V. Evans, Trapped modes in two-dimensional waveguides, J. Fluid Mech. **229**, 51 (1991).

[41] C. H. Retzler, Trapped modes: An experimental investigation, Applied Ocean Research **23**, 249 (2001).

[42] P. J. Cobelli, V. Pagneux, A. Maurel, and P. Petitjeans, Experimental observation of trapped modes in a water wave channel, Europhys. Lett. **88**, 20006 (2009).

[43] P. J. Cobelli, V. Pagneux, A. Maurel, and P. Petitjeans, Experimental study on water-wave trapped modes, J. Fluid Mech. **666**, 445 (2011).

[44] J. Gomis-Bresco, D. Artigas, and L. Torner, Anisotropy-induced photonic bound states in the continuum, Nat. Photonics **11**, 232 (2017).

[45] S. Mukherjee, J. Gomis-Bresco, P. Pujol-Closa, D. Artigas, and L. Torner, Topological properties of bound states in the continuum in geometries with broken anisotropy symmetry, Phys. Rev. A **98**, 063826 (2018).

[46] C. Wei Hsu, B. Zhen, A. Douglas Stone, J. D. Joannopoulos, and Marin Soljačić, Bound states in the continuum, Nat. Rev. Mater. **1**, 16048 (2016).

[47] E. N. Bulgakov and D. N. Maksimov, Topological Bound States in the Continuum in Arrays of Dielectric Spheres, Phys. Rev. Lett. **118**, 267401 (2017).

[48] Y.-X. Xiao, G. Ma, Z.-Q. Zhang, and C. T. Chan, Topological Subspace-Induced Bound State in the Continuum, Phys. Rev. Lett. **118**, 166803 (2017).

[49] Y. Zhang, A. Chen, W. Liu, C. Wei Hsu, B. Wang, F. Guan, X. Liu, L. Shi, L. Lu, and J. Zi, Observation of Polarization Vortices in Momentum Space, Phys. Rev. Lett. **120**, 186103 (2018).

[50] H. M. Doeleman, F. Monticone, W. den Hollander, A. Alù, and A. Femius Koenderink, Experimental observation of a polarization vortex at an optical bound state in the continuum, Nat. Photonics **12**, 397 (2018).

[51] M. Takeichi and S. Murakami, Topological Linelike bound states in the continuum, Phys. Rev. B **99**, 035128 (2019).

[52] H. Friedrich and D. Wintgen, Interfering resonances and bound states in the continuum, Phys. Rev. A **32**, 3231 (1985).

[53] H. A. Haus, *Waves and Fields in Optoelectronics* (Prentice Hall, Englewood Cliffs, NJ, 1983).

[54] W. Suh, Z. Wang, and S. Fan, Temporal coupled-mode theory and the presence of non-orthogonal modes in lossless multimode cavities, IEEE J. Quantum Electron. **40**, 1511 (2004).

[55] F. Alpeggiani, N. Parappurath, E. Verhagen, and L. Kuipers, Quasinormal-Mode Expansion of the Scattering Matrix, Phys. Rev. X **7**, 021035 (2017).

[56] M. Deubel, G. von Freymann, M. Wegener, S. Pereira, K. Busch, and C. M. Soukoulis, Direct laser writing of three-dimensional photonic-crystal templates for telecommunications, Nat. Mater. **3**, 444 (2004).

[57] A. Blanco, E. Chomski, S. Grabtchak, M. Ibisate, S. John, S. W. Leonard, C. Lopez, F. Meseguer, H. Miguez, J. P. Mondia, G. A. Ozin, O. Toader, and H. M. van Driel, Large-scale synthesis of a silicon photonic crystal with a complete three-dimensional bandgap near 1.5 micrometres, Nature (London) **405**, 437 (2000).

[58] S. Fan, W. Suh, and J. D. Joannopoulos, Temporal coupled-mode theory for the Fano resonance in optical resonators, J. Opt. Soc. Am. A **20**, 569 (2003).

[59] C. Wei Hsu, B. Zhen, M. Soljačić, and A. Douglas Stone, Polarization state of radiation from a photonic crystal slab, arXiv:1708.02197.

[60] S. G. Johnson, S. Fan, P. R. Villeneuve, J. D. Joannopoulos, and L. A. Kolodziejski, Guided modes in photonic crystal slabs, Phys. Rev. B **60**, 5751 (1999).

[61] A. F. Oskooi, D. Roundy, M. Ibanescu, P. Bermel, J. D. Joannopoulos, and S. G. Johnson, Meep: A flexible free-software package for electromagnetic simulations by the FDTD method, Comput. Phys. Commun. **181**, 687 (2010).

[62] See Supplemental Material at http://link.aps.org/supplemental/10.1103/PhysRevLett.123.023902 for a discussion of the phase jump of D across lines of BICs and a demonstration that the systems discussed here realize true BICs with $D = 0$, and not simply high-Q resonances.

[63] S. G. Johnson and J. D. Joannopoulos, Block-iterative frequency-domain methods for Maxwells equations in a planewave basis, Opt. Express **8**, 173 (2001).

[64] H. Zhou, C. Peng, Y. Yoon, C. Wei Hsu, K. A. Nelson, L. Fu, J. D. Joannopoulos, M. Soljačić, and B. Zhen, Observation of bulk Fermi arc and polarization half charge from paired exceptional points, Science **359**, 1009 (2018).

[65] A. A. Mailybaev, O. N. Kirillov, and A. P. Seyranian, Geometric phase around exceptional points, Phys. Rev. A **72**, 014104 (2005).

[66] F. Li, X. Huang, J. Lu, J. Ma, and Z. Liu, Weyl points and Fermi arcs in a chiral phononic crystal, Nat. Phys. **14**, 30 (2018).

[67] B. Xie, H. Liu, H. Cheng, Z. Liu, S. Chen, and J. Tian, Experimental Realization of Type-II Weyl Points and Fermi Arcs in Phononic Crystal, Phys. Rev. Lett. **122**, 104302 (2019).